Group-velocity self-matching of femtosecond pulses in noncollinear parametric generation

P. Di Trapani and A. Andreoni
Istituto di Scienze Matematiche, Fisiche e Chimiche, Università degli Studi di Milano, Via Lucini 3, 22100 Como, Italy

G. P. Banfi and C. Solcia
Dipartimento di Elettronica, Università di Pavia, Via Abbiategrasso 209, 27100 Pavia, Italy

R. Danielius and A. Piskarskas
Laser Research Center, University of Vilnius, Sauletekio avenue 10, 2054 Vilnius, Lithuania

P. Foggi
European Laboratory for Nonlinear Spectroscopy, Largo Enrico Fermi 2, 50125 Firenze, Italy

M. Monguzzi
Laser and Lidar Section, Centro Informazioni Studi Esperienze, Via Reggio Emilia 39, 20090 Segrate (MI), Italy

C. Sozzi
Centro Elettronica Quantistica e Strumentazione Elettronica-Consiglio Nazionale delle Ricerche, Politecnico di Milano, Piazza Leonardo da Vinci 32, 20133 Milano, Italy

(Received 27 July 1994)

We show that the parametric superfluorescence generated by a 200-fs pulse at 0.6 μm in a β-barium borate crystal occurs in directions, and at wavelengths, that minimize the group-velocity mismatch between pump and generated pulses. Favorable conditions for generation of tunable femtosecond pulses are found in noncollinear phase matching, a geometry of interaction which is worth exploiting in parametric devices.

PACS number(s): 42.65.Ky, 42.60.—v, 42.79.Nv, 42.25.Md

I. INTRODUCTION

Three-wave optical parametric interaction in media with a second-order nonlinear susceptibility is an efficient way to generate and amplify tunable radiation (for an overview of the subject see [1–3]). During parametric amplification, energy is transferred from the pump to the signal and idler waves, as we define the three waves in order of decreasing frequencies. The amplified quantum noise [4–6], which is observed in the absence of signal (or idler) input and with a condition of high gain, is usually called parametric superfluorescence.

The angular intensity distribution and the related spectrum of superfluorescence carry the imprints of the parametric amplification at the various signal and idler wave vectors $\mathbf{k}_s$ and $\mathbf{k}_i$. When spatial walk-off [3] and group-velocity (GV) mismatch can be neglected [19], the intensity distribution and spectrum are determined by four main phenomena: (i) the dependence of the amplification on the length over which the pump, signal, and idler beams overlap; (ii) the dependence of the effective crystal nonlinearity on the angles of interaction; (iii) the dependence of the gain factor on the signal and idler frequencies; and (iv) the dependence of the amplification on crystal absorption and thus on the wavelengths of the generated pulses. In such a case, parametric superfluorescence shows a smooth angular intensity distribution, typically peaked at a few degrees from the pump beam [7]. When walk-off and GV mismatch play a role, it is convenient to introduce two critical lengths: the signal (idler) beam-splitting length ℓ_s (ℓ_i) that is the distance at which, in the absence of interaction, the signal (idler) beam separates from the pump beam due to the effect of the spatial walk-off, and the pulse-splitting length l_s (l_i) that is the distance at which the signal (idler) pulse separates from the pump pulse due to GV mismatch. When the pump beam is so narrow that ℓ_s or ℓ_i is shorter than the crystal, the effect of the walk-off becomes relevant and the largest amplification tends to take place at noncollinear directions that maximize the overlapping of the Poynting vectors of the interacting beams, as calculated by Dou, Josse, and Zyss [8] and observed by Schroder [9]. In the case of ultrashort pulses (e.g., l_s or l_i shorter than the crystal), a role similar to that of the walk-off should be played by the GV mismatch: when GV mismatch causes a noticeable (longitudinal) lag of one pulse behind the other along the crystal, the highest parametric amplification should take place for those $\mathbf{k}_s$ and $\mathbf{k}_i$ that maximize the temporal overlapping of the pulses. The observation of a drift in the central wavelength when changing the length of a synchronously pumped optical parametric resonator [10] and the off-axis parametric emission recently noticed with femtosecond pulses [11–14] can be considered as previous indications of the relevance of the GV matching requirement.

In this work we show that, for the typical operating conditions of femtosecond, traveling-wave parametric generators, the constraints imposed by the synchronism

of the GV's dominate the other effects: the angular intensity distribution and the spectral features of the parametric superfluorescence can be fully ascribed to a phenomenon of GV self-matching among the interacting pulses.

II. EXPERIMENTAL RESULTS

The pump pulses were generated by a synchronously pumped dye laser, amplified at a 30-Hz repetition rate, spatially filtered, and then collimated to a beam of ≈ 0.7 mm full width at half maximum (FWHM) diameter. Other pulse parameters were 200 fs FWHM duration, 0.6 μm wavelength, 120 cm^{-1} spectral width, beam divergence ≈ 1.3 larger than diffraction limited, and 40 μJ pulse energy. The experimental results were obtained employing a 8-mm-long β-barium borate (BBO) crystal cut at 28° (angle between normal to entrance face and crystal axis) operated in phase-matching II, i.e., with crossed polarization for signal and idler. The geometry and the relevant angles are shown in Fig. 1. With our pump wavelength, BBO can generate superfluorescence in the wavelength range $\lambda_s = 0.74-1.2$ μm ($\lambda_i = 1.2-3.1$ μm), the limit being dictated by the crystal absorption of the idler that rapidly increases at wavelengths greater than 2.5 μm [15].

Measurements of the signal intensity distribution on a vertical screen perpendicular to the pump direction (Fig. 1) showed that the emission was sharply favored along a cone-shaped surface around the pump beam, but not symmetric with respect to it. The angular aperture of this cone decreased at decreasing α and, for $\alpha \approx 23°$, which corresponds to the edge of the tuning in collinear configuration ($\lambda_s = 0.74$ μm and $\lambda_i = 3.1$ μm), the "ring" on the screen collapsed into a spot. Quantitative measurements of the far-field intensity distribution were performed with a diode array (Reticon, 1024 pixels) placed in the focal plane of an $f = 100$ mm positive lens (acceptance angle $\theta_{ext} = \pm 9°$) and filters. Intensity angular distributions of the signal superfluorescence, as detected in the horizontal plane containing both the pump beam and the crystal axis, are shown in Fig. 2 for $\alpha = 28.8°$ 26.9°, and 24.3°. The distributions appear to be peaked at two

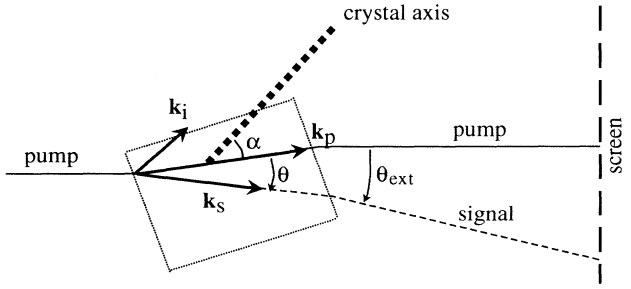

FIG. 1. Geometry adopted for noncollinear parametric generation (horizontal plane) showing the wave vectors $\mathbf{k}_p$, $\mathbf{k}_s$, and $\mathbf{k}_i$ of pump, signal, and idler, respectively. The pump axis (parallel to $\mathbf{k}_p$), the pump electric field, and the BBO-crystal axis lie in the plane of the figure. The angle α is changed by rotating the crystal in the horizontal plane.

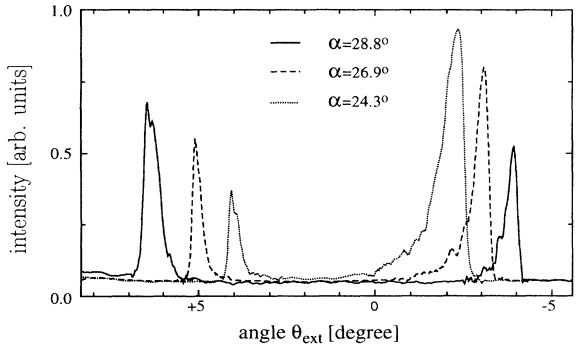

FIG. 2. Angular distribution of the signal intensity, in the horizontal plane, as a function of θ_{ext} for three values of α.

well-defined θ_{ext} values of opposite signs. We call θ_+ and θ_- the corresponding angles inside the crystal. A plot of the values of θ_+ and θ_- vs α is given in Fig. 3(a) (squares). Note that the mentioned limitation on the acceptance angle of the detection apparatus sets the upper limit to the values of α in Fig. 3(a). The spectrum of the signal emitted at all directions along the cone was measured with a spectrometer equipped with an optical multichannel analyzer (OMA). The spectra obtained for two different values, $\alpha = 27.4°$ and 26.2°, are plotted in Fig. 4. They are not corrected for the spectral response of the detection. The signal spectrum shifts to longer wavelengths at increasing α. Spectra at larger α were not ac-

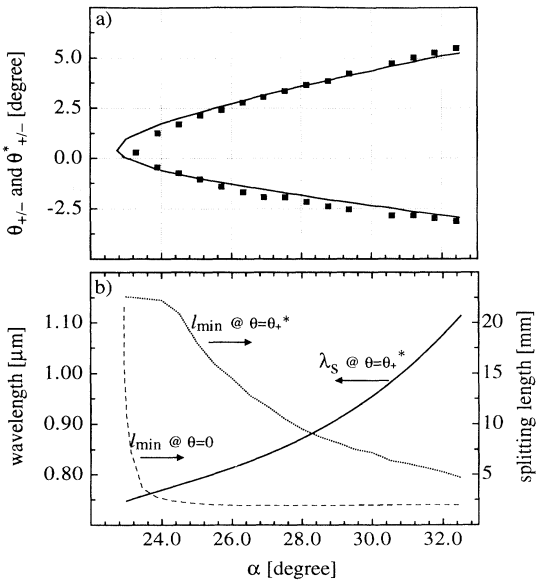

FIG. 3. (a) Experimental values θ_+ and θ_- at which the peaks of the signal occur, in the horizontal plane, as a function of α (squares). Calculated angles θ_+^* and θ_-^* of minimum GV mismatch (full line). (b) Calculated pulse-splitting length $l_{min} = \min\{l_s, l_i\}$ for $\theta = 0$ and $\theta = \theta_+^*$ (right scale), and calculated signal wavelength λ_s at $\theta = \theta_+^*$ (left scale) as a function of α. For $\theta = 0$, $l_{min} = |l_i|$.

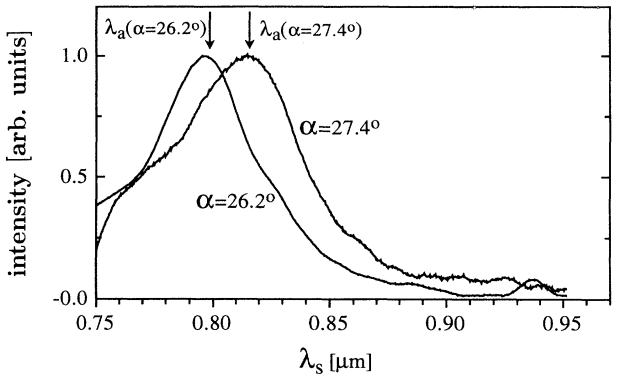

FIG. 4. Detected spectra of the signal emitted in all of the cone for two values of α. The arrows denote the expected average wavelengths $\lambda_a=[\lambda_s(\theta=\theta_+)+\lambda_s(\theta=\theta_-)]/2$.

quired due to the drop in the OMA sensitivity above 0.9 μm. The energy of the superfluorescence (idler plus signal pulses) was estimated from pump-depletion measurements and turned out to be 2–4 μJ, depending on α, which corresponds to a total conversion efficiency of 5–10 %.

III. DISCUSSION

A simple model based on the concept that the smaller the GV mismatch, the higher the parametric amplification, accounts well for both wavelengths and directions of the observed superfluorescence. According their definitions, the pulse-splitting lengths are given by the expression

$$l_j=\frac{\tau}{\left[\frac{1}{v_j}-\frac{1}{v_p}\right]}\ ,\quad j=s,i \tag{1}$$

in which τ is the FWHM pulse duration and $v_{s,i}$ are the GV components along $\mathbf{k}_p$. In the horizontal plane (Fig. 1) and for arbitrary α, we calculated l_s and l_i as a function of θ, i.e., the angle at which the signal propagates, and considered the quantity $l_{\min}(\theta)=\min\{|l_s(\theta)|,|l_i(\theta)|\}$. It exhibits two maxima at two angles of opposite signs, θ_+^* and θ_-^*, that allow the best synchronism among the pulses. The values of θ_+^* and θ_-^* are plotted in Fig. 3(a) (full line) as a function of α. The comparison with the experimental θ_+ and θ_- shows a good agreement for almost all the α's, thus proving that, in our experimental conditions, a self-matching of GV's occurs. Some competition between the roles of GV self-matching and crystal absorption seems to take place close to the tuning edge, i.e., when α approaches 23°. In fact, a discrepancy is observed in Fig. 3(a) at $\alpha<25°$, where the wavelengths of the idler pulses that would experience the best GV matching fall in the BBO absorption band: since $\lambda_i>2.5$ μm for $\alpha<25°$ [cf., the calculated $\lambda_s(\alpha)$ at $\theta=\theta_+^*$, full line in Fig. 3(b)], it is likely that experimental values of θ_+ lower than the calculated ones, θ_+^* are found because they allow shorter idler wavelengths. In addition, the fact that this range of α values is the only one where $l_{\min}(\alpha)$ shows sizable values, even in collinear configuration [dashed line in Fig. 3(b)], can also play some role in making the requirement of GV matching less stringent.

Plotting the values of $l_{\min}$ calculated at $\theta=\theta_+^*$ as a function of α [dotted line in Fig. 3(b)] provides evidence that the noncollinear pulse-splitting lengths are several times larger than the collinear ones [see dashed line in Fig. 3(b)] and, for most α's longer than the crystal itself. We show in the following that this allows noncollinear parametric amplification larger by some orders of magnitude than the collinear one in a broad tuning range. It also accounts for the shape of the signal-wave intensity profiles in Fig. 2 and the observed high contrast between noncollinear and collinear signals. The calculations were performed for the case $\alpha=26.9°$ and for θ equal to either $\theta_+(\alpha)$ or 0. In the noncollinear case, from the plot of $l_{\min}(\alpha)$ in Fig. 3(b), one can see that the pulse-splitting lengths at $\alpha=26.9°$ are considerably longer than the crystal length; thus the effects of GV mismatch can be neglected in the calculation of the amplification G [12], and an analytical expression for G is then obtained by solving the classical equations of stimulated parametric amplification [1–3]. Under the assumptions of a monochromatic pump, infinite plane waves, ideal phase matching, and the absence of both pump depletion and crystal absorption, one gets

$$G=\cosh^2(\Gamma_0 L)\ , \tag{2}$$

in which L is the crystal length and

$$\Gamma_0=\sqrt{2}d_{\text{eff}}\frac{\sqrt{\omega_s\omega_i\Phi_p}}{\sqrt{\varepsilon_0 n_s n_i n_p c^3}}\ , \tag{3}$$

the n's being the refractive indexes at the frequencies ω_s, ω_i, and ω_p, Φ_p, the pump intensity, and d_{eff} the effective second-order susceptibility for the specific directions of propagation and polarization of the waves. We notice that the weak dependence of Γ_0 on θ through ω_s, ω_i, and d_{eff}, which was shown to account for the off-axis generation observed with subnanosecond pulses [7], is far from explaining the sharp angular intensity distribution in Fig. 2. The averaged value of Γ_0 over the solid angle and frequency range we detected is then used in Eq. (2) for a rough evaluation of the parametric amplification that an input pulse should experience. For a pump intensity $\Phi_p=33$ GW/cm^2, i.e., the estimated peak intensity of our pulse under the assumptions of a Gaussian time profile and Gaussian beam, and from the data in [16], we find $\Gamma_0=18$ cm^{-1} and hence $G\approx10^{12}$ for $L=8$ mm. As shown in Refs. [4–6] superfluorescence generation can be accounted for by stimulated parametric amplification seeded by the quantum noise. The output signal intensity can be found by integrating the output signal intensity per mode, $\Phi_s(\mathbf{k}_s)$, over both solid angle and frequency range detected,

$$\Phi_s(\mathbf{k}_s)=\Phi_{\text{ZP}}(\mathbf{k}_s)[G(\mathbf{k}_s)-1]\ , \tag{4}$$

where Φ_{ZP} is the equivalent noise intensity due to the zero-point fluctuations. Neglecting the dependence of G on $\mathbf{k}_s$ in Eq. (4) and taking for G the value 10^{12} and for Φ_{ZP} the value corresponding to one photon per mode [4–6], one gets an output signal intensity of 10^{10} W/cm^2. Notice that, if one assumes that time and space profiles of the signal pulse are the same as those of the pump, a measured conversion efficiency between 5% and 10% would correspond to a signal peak intensity value only lower by a factor of 4 to 8 than that evaluated by the crude calculation above. A better estimation should consider the dependence of G on $\mathbf{k}$, as well as the role of walk-off and pump depletion.

The calculation of the amplification in the collinear case ($\theta=0$) must take into account the role of GV mismatch, because $l_{\min}$ is generally shorter than the crystal length [see Fig. 3(b), dashed line: $l_{\min}\approx 2$ mm for $\alpha>25°$]. The amplification process can then be described only by numerically solving the pertinent equations [2,12]. The results confirm that when $l_{\min}\geq L$, the peak amplification G is well approximated by Eq. (2), while its value rapidly drops as $l_{\min}$ becomes shorter. For our experimental conditions, we find $G\approx 10^9$, which is lower by three orders of magnitude than the value calculated for noncollinear generation.

Also the special features in Fig. 4 are consistent with results of our calculation given in Fig. 3, though the tuning range in Fig. 4 is limited due to the relatively narrow range of α considered. For the α angles in Fig. 4, our calculations yield $\lambda_s(\theta=\theta_+)=0.83$ μm and $\lambda_s(\theta=\theta_-)=0.77$ μm at $\alpha=26.2°$, and $\lambda_s(\theta=\theta_+)=0.86$ μm and $\lambda_s(\theta=\theta_-)=0.78$ μm at $\alpha=27.4°$. The average values $\lambda_a=[\lambda_s(\theta=\theta_+)+\lambda_s(\theta=\theta_-)]/2$, denoted by the arrows in Fig. 4, fit the peaks of the space-integrated spectra, in agreement with the fact that $\lambda_s(\theta=\theta_+)$ and $\lambda_s(\theta=\theta_-)$ should be the maximum and minimum wavelengths, respectively, in the cone-shaped signal emission.

IV. CONCLUSIONS

The reported results show that noncollinear geometry can solve the problem of GV mismatch in the parametric generation of ultrashort tunable pulses. In fact, from the values of $l_{\min}(\alpha)$ and $\lambda_s(\alpha)$ at $\theta=\theta_+^*$ [see Fig. 3(b)], it is evident that splitting lengths of great practical relevance can be obtained over most of the tuning range. The effects of GV are relevant for the performances (and design criteria) of parametric devices in the ultrashort pulse regime. Their role is crucial in synchronously pumped parametric oscillators [17,18] and even more crucial in the case of traveling-wave parametric generators (TOPG's) [11–13], since they require higher amplifica- tions and, thus, longer crystals. Recently, some of the present authors showed that TOPG's can be operated with 200-fs pump pulses at 0.6 μm by employing a BBO crystal in collinear phase matching, obtaining nearly bandwidth-limited pulses [12,13]. Nevertheless, this result, as well as the simulations in the present paper, indicate that with the usual collinear configuration, serious problems would arise with pump pulses of shorter wavelength and time duration. For example, with 100-fs pump pulses at 0.4 μm (e.g., second harmonics of amplified Ti:sapphire lasers) the collinear pulse-splitting length in BBO would not exceed 0.5 mm. On the other hand, attempts to recover high collinear gains by increasing the intensity suffer from pump depletion due to the off-axis superfluorescence and from pulse distortion due to third-order nonlinear processes.

Based on the results presented here, we expect larger improvements by adopting a noncollinear geometry and choosing the most suitable α and θ values according to the desired λ_s. Preliminary calculations have shown that pulse-splitting lengths larger than 5 mm can be obtained with BBO I (0.4 μm, 100-fs pump), while the signal and idler wavelengths sweep the whole range allowed by the crystal transparency. Experiments in this pump-pulse regime are in progress.

ACKNOWLEDGMENTS

This work has been supported by contracts with the European Community, GE1*CT920046 and ERBCHRXCT930105. The authors thank Dr. Gintaras Valulis (Laser Research Center, University of Vilnius) for his help with numerical calculations.

[1] A. Laubereau, in *Ultrashort Laser Pulses,* edited by V. Kaiser (Springer-Verlag, Berlin, 1988), p. 35.
[2] R. Danielius, A. Piskarskas, V. Sirutkaitis, A. Stabinis, and J. Jasevicjoute, *Optical Parametric Oscillators and Picosecond Spectroscopy,* edited by A. Piskarskas (Mokslas, Vilnius, 1983) (in Russian).
[3] S. J. Brosnan and R. L. Byer, IEEE J. Quantum Electron. **QE-15**, 415 (1979).
[4] T. G. Giallorenzi and C. L. Tang, Phys. Rev. **166**, 225 (1968).
[5] D. A. Kleinman, Phys. Rev. **174**, 1027 (1968).
[6] C. L. Tang, in *Quantum Electronics: a Treatise,* edited by H. Rabin and C. L. Tang (Academic, New York, 1975), Vol. 1A.
[7] A. Lukshas, A. Piskarskas, V. Smilgevicius, and G. Shlekis, Kvant. Elektron. (Moscow) **15**, 2100 (1988) [Sov. J. Quantum Electron. **18**, 1318 (1988)].
[8] S. X. Dou, D. Josse, and J. Zyss, J. Opt. Soc. Am. B **9**, 1312 (1992).
[9] B. Schroder, Opt. Commun. **49**, 75 (1984).
[10] D. C. Edelstein, E. S. Wachman, and C. L. Tang, Appl. Phys. Lett. **54**, 1728 (1989).
[11] W. Joosen, H. J. Bakker, L. D. Noordman, H. G. Muller, and H. B. van Linden van den Heuvell, J. Opt. Soc. Am. B **8**, 2087 (1991).
[12] R. Danielius, A. Piskarskas, A. Stabinis, G. P. Banfi, P. Di Trapani, and R. Righini, J. Opt. Soc. Am. B **10**, 2222 (1993).

[13] G. P. Banfi, P. Di Trapani, R. Danielius, A. Piskarskas, R. Righini, and I. Sa'nta, Opt. Lett. **18**, 1547 (1993).

[14] P. Di Trapani, G. P. Banfi, R. Danielius, P. Foggi, M. Monguzzi, A. Piskarskas, R. Righini, I. Sa'nta, and C. Sozzi, in Proceedings of the Eighth International Symposium on Ultrafast Processes in Spectroscopy—UPS '93, Vilnius, Lithuania [Liet. Fiz. Zurnalas **33**, 324 (1993)].

[15] D. Eimerl, L. Davis, S. Velsko, E. K. Graham, and A. Zalkin, J. Appl. Phys. **62**, 1968 (1987).

[16] Data on BBO from Data Sheet, *Beta Barium Borate: Basic Properties, Advantages, and Major Applications* (Fujian Castech Crystals, Inc., Fuzhou, Fujian, China, 1994).

[17] R. Laenen, H. Graener, and A. Laubereau, Opt. Lett. **17**, 971 (1990).

[18] R. Laenen, K. Wolfrum, A. Seilmeier, and A. Laubereau, J. Opt. Soc. Am. B **10**, 2151 (1993).

[19] The spatial walk-off is defined as the lack of parallelism between the **k** vector and the Poynting vector; it occurs for extraordinary waves in birefringent media. In general, in phase-matching conditions, the walk-off prevents the Poynting vectors of idler, signal, and pump fields from having the same direction and, in the absence of parametric interaction, the beams from overlapping over a long path in the crystal. The group-velocity mismatch between pulses with different wavelengths and/or polarizations due to dispersion introduces a lap among the pulses which also limits the pathlength of overlap. Note that the modifications in beam and pulse profiles due to the parametric interaction affect the pathlength over which the interaction can occur.